AIMS Mathematics, 6(3): 2468–2485.
DOI: 10.3934/math.2021150
Received: 27 September 2020
Accepted: 09 December 2020
Published: 21 December 2020

http://www.aimspress.com/journal/Math

Research article

Neuro-swarms intelligent computing using Gudermannian kernel for solving a class of second order Lane-Emden singular nonlinear model

Zulqurnain Sabir[1], Muhammad Asif Zahoor Raja[2,3], Adnène Arbi[4], Gilder Cieza Altamirano[5], Jinde Cao[6,7,*]

[1] Department of Mathematics and Statistics, Hazara University, Mansehra, Pakistan
[2] Future Research Technology Center, National Yunlin University of Science and Technology, 123 University Road, Section 3, Douliou, Yunlin 64002, Taiwan, R.O.C.
[3] Department of Computer and Electrical Engineering, COMSATS University Islamabad, Attock Campus, Attock 43600, Pakistan
[4] Department of Advanced Sciences and Technologies at National School of Advanced Sciences and Technologies of Borj Cedria; Laboratory of Engineering Mathematics (LR01ES13), Tunisia Polytechnic School, University of Carthage, Tunisia
[5] Department of General Studies, National Autonomous University of Chota, Perú
[6] School of Mathematics, Southeast University, Nanjing, China
[7.] Yonsei Frontier Lab, Yonsei University, Seoul, Korea

*** Correspondence**: Email: jdcao@seu.edu.cn; Tel: +862552090588.

Abstract: The present work is to design a novel Neuro swarm computing standards using artificial intelligence scheme to exploit the Gudermannian neural networks (GNN)accomplished with global and local search ability of particle swarm optimization (PSO) and sequential quadratic programming scheme (SQPS), called as GNN-PSO-SQPS to solve a class of the second order Lane-Emden singular nonlinear model (SO-LES-NM). The suggested intelligent computing solver GNN-PSO-SQPS using the Gudermannian kernel are unified with the configuration of the hidden layers of GNN of differential operators for solving the SO-LES-NM. An error based fitness function (FF) applying the differential form of the differential model and corresponding boundary conditions. The FF is optimized together with the combined heuristics of PSO-SQPS. Three problems of the SO-LES-NM are solved to validate the correctness, effectiveness and competence of the designed GNN-PSO-SQPS. The performance of the GNN-PSO-SQPS through statistical operators is tested to check the constancy, convergence and precision.

Keywords: Lane-Emden singular system; Gudermannian neural networks; Sequential quadratic scheme; Gudermannian kernel; Numerical results; Particle swarm optimization.

Mathematics Subject Classification: 68T20, 65Lxx, 68U99

1. Introduction

The singular based models have gotten much importance due to its valued applications in physiology, physics and mathematics submissions. The Lane-Emden based model is one the historic paramount singular model introduced by famous astrophysics Lane and the further explored by Emden [1,2]. The general form of the second order Lane-Emden singular nonlinear model (SO-LES-NM) is given as [3]:

$$\begin{cases} v''(\eta)+\dfrac{\sigma}{\eta}v'(\eta)+g(\eta,v)=0,\ ,\ \sigma\geq 0,\ 0<\eta\leq 1, \\ v(0)=i_1,\ v'(0)=i_2, \end{cases} \tag{1}$$

where i_1 and i_2 are constants, σ is the shape factor, while $g(\eta,v)$ is known as the real valued continuous function.

The singular Lane-Emden nonlinear systems are widely implemented to solve an assortment of phenomena in the fields of physical science [4], gaseous star density [5], electromagnetic theory [6], morphogenesis study [7], stellar structure model [8], study of mathematical physics [9], oscillating magnetic fields [10], dusty fluid system [11] and an isotropic standard [12]. The singular models due to singularity are found to be hard and grim at the origin. A small number of numerical and analytical approaches are available to tackle such nonlinear singular systems are given in these references [13–16].

All above-mentioned approaches shave their specific sensitivity, efficiency, potential and perfection, as well as, weaknesses, disadvantages, imperfections, flaws and demerits over one another. The potential of the wide-ranging computing heuristic of the scheme is applied to the singular models using the extensive approximation aptitude of artificial neural networks (ANNs) mutually with the local and global methodologies [17–23]. Some notable illustrations contain mosquito dispersal study in a heterogeneous conditions [24], nonlinear dusty plasma system [25], nonlinear functional differential singular models[26,27], plasma physics studies [28], Thomas-Fermi system [29], HIV infection system of CD4+ T cells [30], biological prey-predator model [31], nonlinear singular periodic differential system [32],nanotechnology systems [33], Jeffery Hamel flow problem [34], corneal shape system based on eye surgery [35], singular differential model [36] and atomic physics system [37].

These prospective and potential submissions demonstrated the importance, value and significance of the numerical stochastic based computing solvers in terms of exactitude, stability and convergence. Consequently, the novel features of the Gudermannian neural network (GNN) are designed together with particle swarm optimization (PSO) and the sequential quadratic programming scheme, i.e., GNN-PSO-SQPS to solve the SO-LES-NM.

The motive of this research work is to solve SO-LES-NM by integrating the intelligent computing approach based on the GNN-PSO-SQPS. The innovative features of the GNN-PSO-SQPS are given as follows:

- A novel computingGNN-PSO-SQPSintelligentsolveris exploited and explored using the GNN along with the hybrid-combination of PSO-SQPS.

- The designed GNN-PSO-SQPS are tested precisely and accurately for solving three different problems of the SO-LES-NM.
- The coinciding of the outcomes achieved by the proposed GNN-PSO-SQPS and the exact results demonstrations the correctness of the scheme to solve SO-LES-NM.
- The results through proposed GNN-PSO-SQPS for single/multiple runsvia performance investigations of mean, root mean square error (RMSE), semi inter quartile range(S-I-R), Theil's inequality coefficient (TIC), median and standard deviation certified the competence, consistency, precision, accuracy and correctness of the designed GNN-PSO-SQPS.

The rest parts of this research paper are given as: The methodology is given in Sec 2, the performance indices information is given in Sec 3, the detail of numerical results together with future research clarifications is given in Section 4.

2. Materials and method

In this section, the design of the differential operator GNN is presented to solve the SO-LES-NM. The detail of the differential model, fitness function (FF) and optimization using the suggested PSO-SQPS are provided.

2.1. Proposed procedure: Gudermannian function

The models based on neural network are familiar to provide the reliable, standardized and consistent solutions for a number of applications indifferent fields. In the below modeling, $\hat{v}(\eta)$ represents the obtained outcomes from the GNN-PSO-SQPS together with its nth derivatives are given as:

$$\begin{aligned} \hat{v}(\eta) &= \sum_{k=1}^{m} a_k h(w_k \eta + q_k) \\ \hat{v}^{(\mathrm{n})}(\eta) &= \sum_{k=1}^{m} a_k h^{(\mathrm{n})}(w_k \eta + q_k), \end{aligned} \tag{2}$$

where, *m* and *n* represent the neurons and derivative order, respectively. The activation function is *h*, whereas, a , w and q are the unidentified weight vectors defined as $\boldsymbol{W} = [\boldsymbol{a}, \boldsymbol{w}, \boldsymbol{q}]$, for $\boldsymbol{a} = [a_1, a_2, a_3, ..., a_m]$, $\boldsymbol{w} = [w_1, w_2, w_3, ..., w_m]$ and $\boldsymbol{q} = [q_1, q_2, q_3, ..., q_m]$. The literature form of the Gudermannian function is given as:

$$v(\eta) = 2\tan^{-1}\left(\mathrm{e}^{\eta}\right) - \frac{\pi}{2} \tag{3}$$

The Gudermannian activation function using the above equation becomes as:

$$\begin{aligned} \hat{v}(\eta) &= \sum_{k=1}^{m} a_k \left(2\tan^{-1} e^{(w_k \eta + q_k)} - 0.5\pi\right), \\ \hat{v}(\eta) &= \sum_{k=1}^{m} a_k \left(2\tan^{-1} e^{(w_k \eta + q_k)} - 0.5\pi\right), \\ \hat{v}'(\eta) &= \sum_{k=1}^{m} 2a_k w_k \left(\frac{e^{(w_k \eta + q_k)}}{1 + \left(e^{(w_k \eta + q_k)}\right)^2}\right), \end{aligned} \tag{4}$$

$$\hat{v}''(\eta)=\sum_{k=1}^{m}2a_k {w_k}^2\left(\frac{e^{(w_k\eta+q_k)}}{1+\left(e^{(w_k\eta+q_k)}\right)^2}-\frac{2e^{(w_k\eta+q_k)^3}}{\left(1+\left(e^{(w_k\eta+q_k)}\right)^2\right)^2}\right)$$

To solve the SO-LES-NM, the formulation of FF using the mean squared error metric is written as:

$$\xi_{FIT}=\xi_{FIT-1}+\xi_{FIT-2}, \tag{5}$$

where ξ_{FIT-1} and ξ_{FIT-2} are the unsupervised error functions connected to the SO-LES-NM and relevant conditions of the SO-LES-NM (1) are given as:

$$\xi_{FIT-1}=\frac{1}{N}\sum_{k=1}^{N}\left(\hat{v}''(\eta_k)+\frac{\sigma}{\eta_k}\hat{v}'(\eta_k)+g\left(\eta_k,\hat{v}(\eta_k)\right)\right)^2, \tag{6}$$

$$\xi_{FIT-2}=\frac{1}{2}\left((\hat{v}_0-i_1)^2+\left(\hat{v}_0'-i_2\right)^2\right), \tag{7}$$

where $Nh=1,\ \hat{v}_k=\hat{v}(\eta_k),\ g(\eta_k,\hat{v})=g(\eta_k,\hat{v}(\eta_k))$ and $\eta_k=kh$.

While the networks presented in (6,7), used Gudermannian function (3) and its derivatives as a activation function. Now after learning of the weights of the networks, one can optimize the fitness/cost function in (6,7) and accordingly the solution of system (1) is approximately by proposed methodology.

2.2. Optimization of the network: PSO-SQPS

The capability of the ANNs based optimization models to solve the SO-LES-NM using the designed GNN-PSO-SQPS.

PSO is used as an alteration of the genetic algorithm and work as a global search method [38-39]. PSO is an easy implementation, needs less memory and global search optimization process introduced in the previous century [40]. Recently, PSO is applied in many applications like as Some recent PSO applications are traveling salesman problem [41], SFO-DTC induction motor drive [42], to evaluate the parameters of the reaction kinetic parameters [43], prediction of asphalting precipitation [44], reducing cost and increasing reliability [45] and object detection in autonomous driving [46].

To modify the PSO parameters, the scheme provides optimal iterative solutions, $\boldsymbol{P}_{LB}^{\Phi-1}$ and $\boldsymbol{P}_{GB}^{\Phi-1}$ denote the swarm's position and velocity, written as:

$$\boldsymbol{X}_i^{\,k}=\boldsymbol{X}_i^{\,k-1}+\boldsymbol{V}_i^{\,k-1}, \tag{8}$$

where $\boldsymbol{V_i}$ and $\mathbf{X}_i$ denote the velocity and position, $\Re_1$ and $\Re_2$ are the constant values of the accelerations, while $\Psi\in[0,1]$ shows the weight inertia vector.

In order to perform the rapid convergence, the global PSO approach is hybridized with an appropriate local search scheme taking the PSO results. Therefore, an operative local search scheme named as SQS is executed to regulate the obtained outcomes through the GNN-PSO-SQPS. Some latest applications of SQS are transient heat conduction model [47], geometric optimization of radioactive enclosures [48], nonlinear predictive control model [49], cognitive radio system [50] and optimal management of automated vehicles at intersections [51]. The detail of the optimization

procedure using the hybrid of PSO-SQPS are tabulated in the pseudo code Table 1.

Table 1. Pseudo code for the GNN-PSO-SQPS to solve the SO-LES-NM.

PSO process starts

Step-1: **Start**: Generate the arbitrarily initial swarms and adjust the PSO parameters using the optimoptions.

Step-2:Fitness Scheme: Examine the fit values to each particle in the Eq. (5).

Step-3: **Ranking**: Rank all those element that have minimum standards of the FF.

Step-4: Stopping Measures: Stop, when one of the below condition meets.

- Selected flights
- Fit Level

Move to Step-5

Step-5: Renewal: For the position and velocity, use Eqs (08) and (09).

Step-6: Elevation: Repeat the steps 02-06 until the whole flights are completed.

Step-7: Storage: store the best fit and designated as $\mathbf{W_{PSO}}$.

End of PSO

Start of PSO-SQPS

Inputs: $\mathbf{W_{PSO}}$

Output: Thebest-achievedfit is $\mathbf{W_{PSO\text{-}SQPS}}$ **Initialize:** Use $\mathbf{W_{PSO}}$ as a start point.

Terminate: Stop,when 'ξ_{Fit} = 10^{-20}', TolX = 10^{-21} 'TolCon = TolFun = 10^{-20}', 'MaxFunEvals = 268000' Iteration = 520.

While: Terminate

Fit Assessment: For ξ_{Fit}, Implement the Eq (5)

Adjustments: Invoke the 'fmincon' using the SQS to adjust the values of the weight vector.

Store the fit for the weight vector

Store: Save $\mathbf{W_{PSO\text{-}SQPS}}$, function count, time, ξ_{Fit} and generations for the current run.

End of PSO-SQPS

Data Generations: The process PSO-SQPS repeats 100 times to find a comprehensive data-set of the optimization process for the SO-LES-NM

3. Performance form

The presentation of two different measures for solving the SO-LES-NM are constructed in terms of the RMSE and TIC that are executed to verify the proposed PSO-SQPS, the mathematical notations of these procedures are given as:

$$\text{RMSE}=\sqrt{\frac{1}{n}\sum_{k=1}^{n}\left(v_k-\hat{v}_k\right)^2}, \tag{10}$$

$$\text{TIC}=\frac{\sqrt{\frac{1}{n}\sum_{k=1}^{n}\left(v_k-\hat{v}_k\right)^2}}{\left(\sqrt{\frac{1}{n}\sum_{k=1}^{n}v_k^2}+\sqrt{\frac{1}{n}\sum_{k=1}^{n}\hat{v}_k^2}\right)}. \tag{11}$$

4. Result simulations

The detailed simulation based results of the numerical results through the GNN-PSO-SQPS for the SO-LES-NM are described in this section.

Example1: Consider the SO-LES-NM (1)having exponential function $g(\eta,v)=e^{2v(\eta)}-0.5e^{v(\eta)}$ as:

$$\begin{cases} v''(\eta)+\dfrac{0.5}{\eta}v'(\eta)+(e^{2v(\eta)}-\dfrac{1}{2}e^{v(\eta)})=0,\ \eta\in(0,1), \\ v(0)=\ln(2),\quad v(1)=0. \end{cases} \tag{12}$$

For the Eq (12), the FF becomes as:

$$\xi_{FIT}=\frac{1}{N}\sum_{k=1}^{N}\left(\eta_k\hat{v}''(\eta_k)+0.5\hat{v}'(\eta_k)+\eta_k(e^{2\hat{v}(\eta_k)}-0.5e^{2\hat{v}(\eta_k)})\right)^2+\frac{1}{2}\left(\left(\hat{v}_0-\ln(2)\right)^2+\left(\hat{v}_N\right)^2\right). \tag{13}$$

The true solution of the Eq (12) is $\ln 2-\ln(\eta^2+1)$.

Example 2: Consider the SO-LES-NM (1) involving fifth order nonlinearity for $g(\eta,v)=v^5(\eta)$ as:

$$\begin{cases} v''(\eta)+\dfrac{2}{t}v'(\eta)+v^5(\eta)=0,\ \eta\in(0,1), \\ v(1)=\sqrt{0.75},\quad v'(0)=0. \end{cases} \tag{14}$$

For the Eq (14), the FF becomes as:

$$\xi_{FIT}=\frac{1}{N}\sum_{k=1}^{N}\left(\eta_k\hat{v}''(\eta_k)+2\hat{v}'(\eta_k)+\eta_k\hat{v}^5(\eta_k)\right)^2+\frac{1}{2}\left(\left(\hat{v}_N-0.75\right)^2+\left(\hat{v}_0'\right)^2\right). \tag{15}$$

The true solution takes the form as $\left(\dfrac{3}{\eta^2+3}\right)^{\frac{1}{2}}$.

Example3: Consider the SO-LES-NM (1) involving exponential function $g(\eta,v)=e^{v(\eta)}$ as:

$$\begin{cases} v''(\eta)+\dfrac{1}{\eta}v'(\eta)+e^{v(\eta)}=0,\ \eta\in(0,1), \\ v(1)=v'(0)=0. \end{cases} \tag{16}$$

For the Eq (16), the FF becomes as:

$$\xi_{FIT} = \frac{1}{N}\sum_{k=1}^{N}\left(\eta_k \hat{v}''(\eta_k) + \hat{v}'(\eta_k) + \eta_k e^{\hat{v}(\eta_k)}\right)^2 + \frac{1}{2}\left(\left(\hat{v}_0\right)^2 + \left(\hat{v}_N\right)^2\right). \tag{17}$$

The true solution of the Eq (16) is $\ln\left(\frac{4-2\sqrt{2}}{(3-2\sqrt{2})\eta^2+1}\right)^2$.

The optimization for all the examples of the SO-LES-NM optimized by the hybrid of PSO-SQPS using the Gudermannian activation function for hundred independent runs to get the system variables of the parameter. A set of the best weights authenticate the numerical results by taking 10 neurons and the mathematical notations of these proposed outcomes is written as:

$$\begin{aligned}\hat{v}_1(\eta) = {} & 0.7453(2\tan^{-1}e^{(2.0927\eta+1.1104)} - 0.5\pi) + 0.1109(2\tan^{-1}e^{(-0.801\eta+5.8171)} - 0.5\pi)\\ & + 2.0076(2\tan^{-1}e^{(1.5406\eta+0.3425)} - 0.5\pi) - 2.6674(2\tan^{-1}e^{(2.1168\eta+2.3665)} - 0.5\pi)\\ & - 2.5625(2\tan^{-1}e^{(0.1558\eta-0.0935)} - 0.5\pi) - 0.4081(2\tan^{-1}e^{(1.0143\eta+10.712)} - 0.5\pi)\\ & - 0.7660(2\tan^{-1}e^{(-4.1431\eta-3.0384)} - 0.5\pi) + 1.5666(2\tan^{-1}e^{(-1.2997\eta-0.735)} - 0.5\pi)\\ & - 2.1009(2\tan^{-1}e^{(-1.7895\eta+5.5393)} - 0.5\pi) + 1.7772(2\tan^{-1}e^{(-0.5024\eta+0.599)} - 0.5\pi),\end{aligned} \tag{18}$$

$$\begin{aligned}\hat{v}_2(\eta) = {} & 10.138(2\tan^{-1}e^{(10.799\eta+12.852)} - 0.5\pi) - 12.223(2\tan^{-1}e^{(0.035\eta+1.0954)} - 0.5\pi)\\ & - 11.339(2\tan^{-1}e^{(11.867\eta+9.207)} - 0.5\pi) - 7.1434(2\tan^{-1}e^{(-2.011\eta-4.574)} - 0.5\pi)\\ & - 7.3114(2\tan^{-1}e^{(-2.011\eta-4.574)} - 0.5\pi) - 7.3114(2\tan^{-1}e^{(11.676\eta+9.506)} - 0.5\pi)\\ & - 3.0726(2\tan^{-1}e^{(-2.012\eta-11.384)} - 0.5\pi) + 1.1013(2\tan^{-1}e^{(12.393\eta+11.63)} - 0.5\pi)\\ & + 7.8400(2\tan^{-1}e^{(7.2194\eta+11.870)} - 0.5\pi) + 4.9173(2\tan^{-1}e^{(-8.072\eta-11.27)} - 0.5\pi),\end{aligned} \tag{19}$$

$$\begin{aligned}\hat{v}_3(\eta) = {} & 1.8380(2\tan^{-1}e^{(2.1397\eta+6.8250)} - 0.5\pi) + 8.1775(2\tan^{-1}e^{(-6.0183\eta+7.2965)} - 0.5\pi)\\ & - 6.3058(2\tan^{-1}e^{(-0.779\eta+2.4809)} - 0.5\pi) + 5.9782(2\tan^{-1}e^{(8.4858\eta+7.5846)} - 0.5\pi)\\ & - 4.9626(2\tan^{-1}e^{(0.1227\eta-8.6133)} - 0.5\pi) - 9.4747(2\tan^{-1}e^{(-1.382\eta+6.6550)} - 0.5\pi)\\ & + 6.3056(2\tan^{-1}e^{(-0.328\eta+1.5773)} - 0.5\pi) - 2.3713(2\tan^{-1}e^{(-5.0314\eta-7.622)} - 0.5\pi)\\ & + 1.2986(2\tan^{-1}e^{(5.2289\eta+7.6306)} - 0.5\pi) + 8.9176(2\tan^{-1}e^{(-6.4814\eta-7.933)} - 0.5\pi),\end{aligned} \tag{20}$$

Figure 1 represents the set of the best weights for 10 neurons along with the comparison of the exact, best and mean performances of the results for the SO-LES-NM based Examples 1–3. The value of the best weight sets by using the Eqs 18 to 20 are plotted in the Figure 1 for all the problems. The numerical performances of the exact, best and mean results have been performed between 0 and 1 with the step size 0.1 along with 10numbers of neurons throughout this research study. The comparison of these mentioned exact, best and mean results for all the examples of the SO-LES-NM is matched over one another. These valuations of the outcomes represented in the Figure 1 specify the exactness, perfection and accuracy of the advised GNN-PSO-SQPS. The performance soundings based on the

FIT, RMSE and TIC operators along with the mean, worst and best AE values for all measures of SO-LES-NM is plotted in Figure 2. To investigate the performances for the example 1, one can observe that the best FIT and TIC values lie around 10^{-08} to $10^{-10}$and the best RMSE values exist in10^{-05} to 10^{-06} interval. The mean FIT, RMSE and TIC values for example 1 exist in the ranges of10^{-04} to 10^{-06}, 10^{-03} to 10^{-04} and 10^{-07} to 10^{-08}, respectively. For examples 2 and 3, the best values of the FIT, RMSE and TIC values lie around 10^{-08} to 10^{-10}. The mean values of the FIT, RMSE and TIC values lie around 10^{-02} to 10^{-04}, 10^{-05} to 10^{-06} and 10^{-01} to 10^{-03}. The worst values for all the performance indices are also found in good ranges. Toevaluate the absolute error (AE) for the examples 1, 2 and 3, the best values are calculated around 10^{-05}–10^{-06}, 10^{-04} to 10^{-05} and 10^{-04} to 10^{-06}. The mean gage values are found around 10^{-03} to 10^{-04}, 10^{-01} to $10^{-03}$and 10^{-02} to 10^{-03}, respectively. On the behalf of these indices, one can calculate the specific, accurate and precise values of the RMSE and TIC for all theSO-LES-NM based examples 1 to 3. The statistical investigation based on Fitness, RMSE and TIC values using the histogram and the box plots for the SO-LES-NM is provided in Figures 3 to 5. It is interpreted that most of the independent executions have been achieved best values of FIT, RMSE and TIC.

Statistical representations have been scrutinized applying the GNN-PSO-SQPS to solve the SO-LES-NM for 100 independent executions using the mean, semi inter quartile range (S.I.R), maximum (Max), standard deviation (STD), minimum (Min) and median (MED) are tabulated in Table 2. The Min gage value shows the best outcomes, whereas the Max values show the worst runs for the GNN-PSO-SQPS. S.I.R is one-half of the 3^{rd} and 1^{st} quartile difference. These statistic measures for all examples of the SO-LES-NM are obtained satisfactory. The global demonstrations for all examples of the SO- LES-NM applying the proposed GNN-PSO-SQPS are provided in Table 3. The Min [G-FIT], [G-RMSE] and [G-TIC] values lie 10^{-08} to 10^{-10}, 10^{-05} to 10^{-06} and 10^{-09} to 10^{-10}, respectively, whereas the MED values are examined in the ranges of 10^{-07} to 10^{-08}, 10^{-04} to $10^{-05}$and 10^{-08} to 10^{-09}, respectively for the SO-LES-NM using the designed GNN-PSO-SQPS. These optimal achieved values from the designed GNN-PSO-SQPS based global operatives approve the accuracy of the scheme. The complexity performances for the SO-LES-N Musing the designed GNN-PSO-SQPS based on the iterations, period of executions and function evaluations are provided in Table 4. One can see that the generations values, executed time together with the count of function lie around 35.553778, 1561.16667 and 53176.38667, respectively, for solving the SO-LES-NM using the designed GNN-PSO-SQPS.

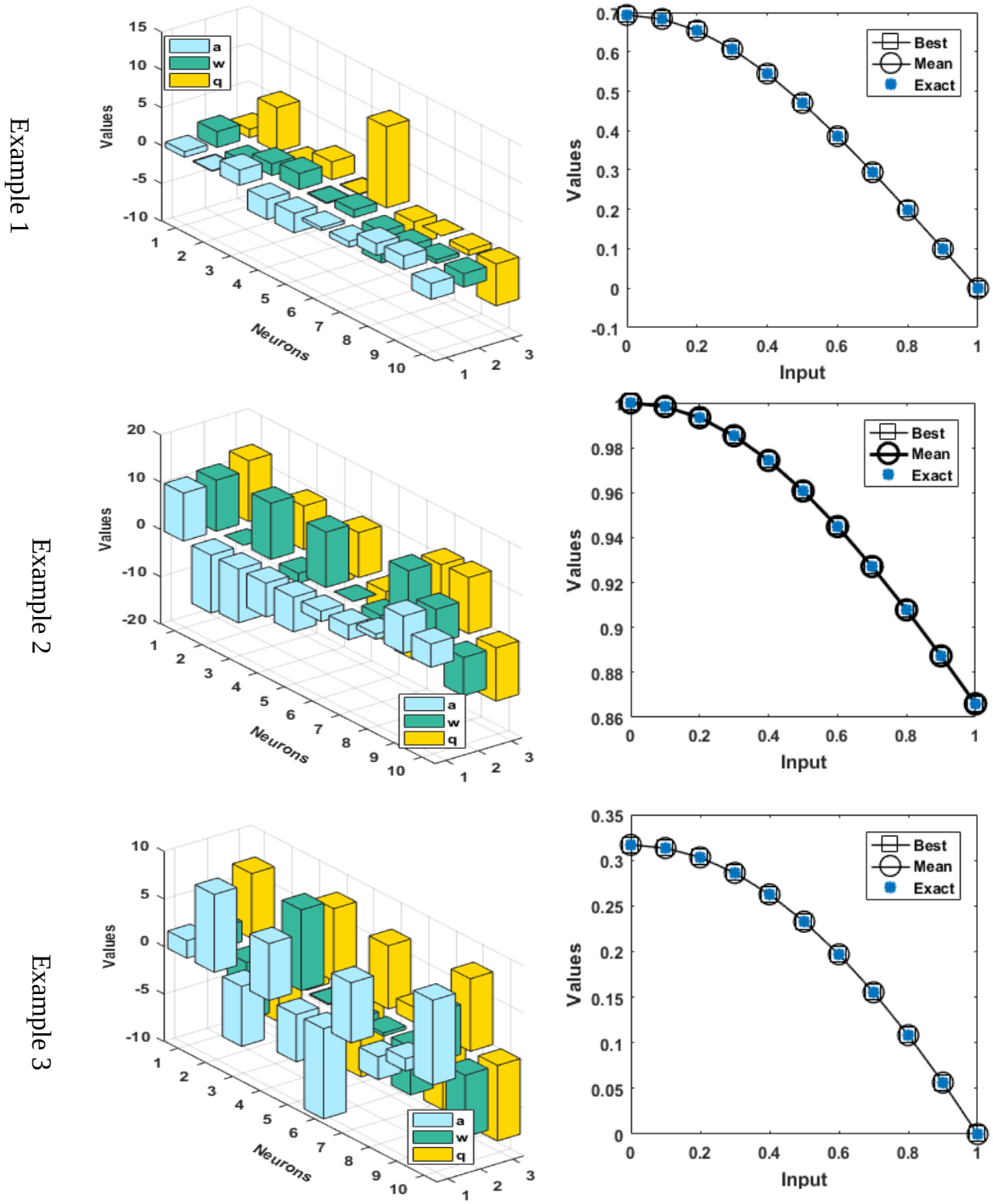

Figure 1. A set of best weights for 10 neurons along with the comparison of the exact, best and mean performances of the results for the SO-LES-NM based Examples 1–3.

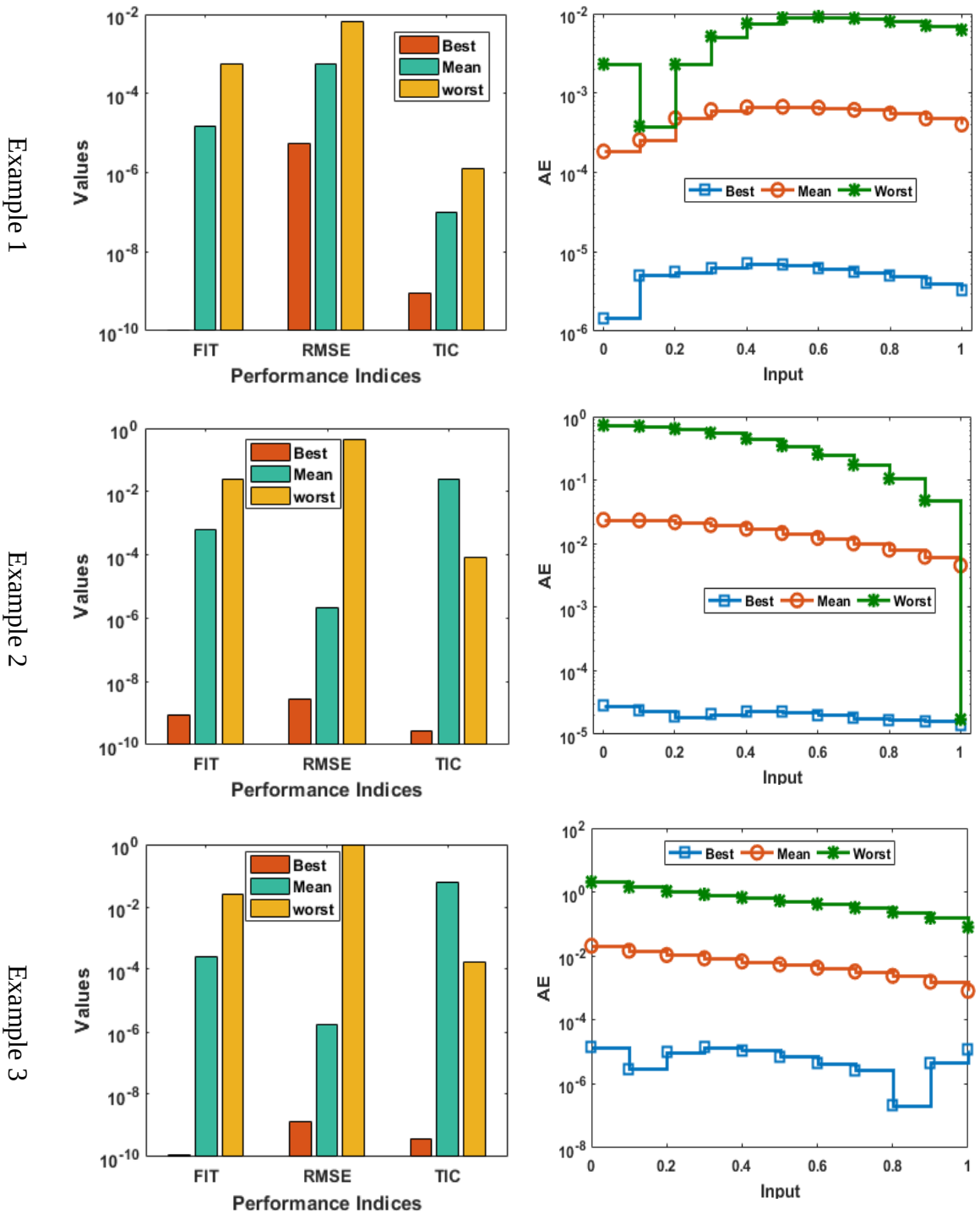

Figure 2. Performance soundings based on the FIT, RMSE and TIC operators along with the mean, worst and best AE values for all the measures of SO-LES-NM.

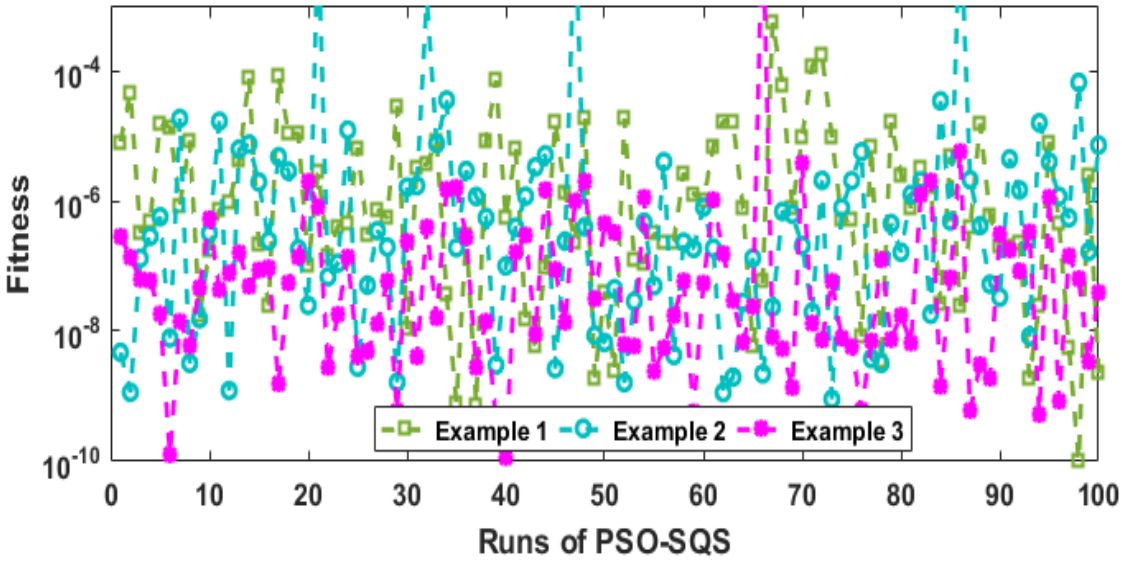

(a) Fitvalues using convergence investigationsfor Examples 1 to 3.

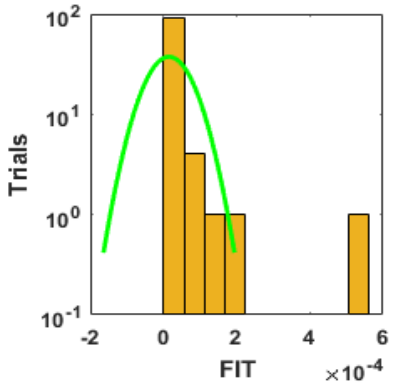

(b) HistforExample1

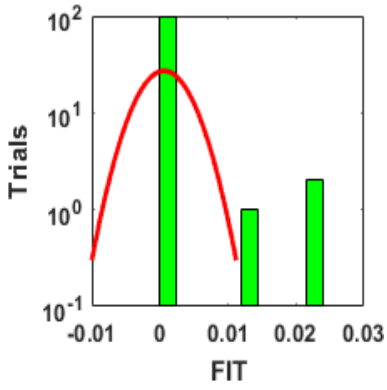

(c) Hist for Example 2

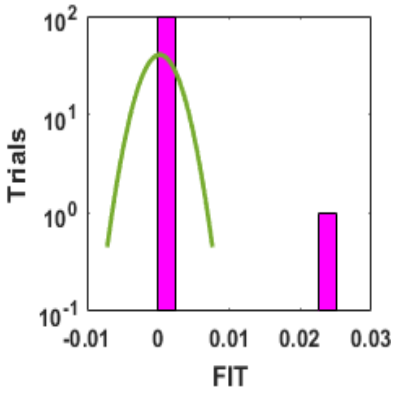

(d) Hist for Example 3

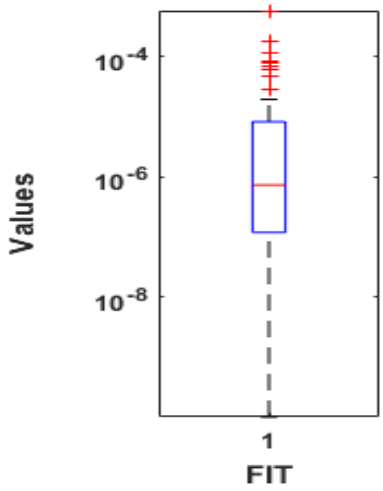

(e) Boxplot: Example 1

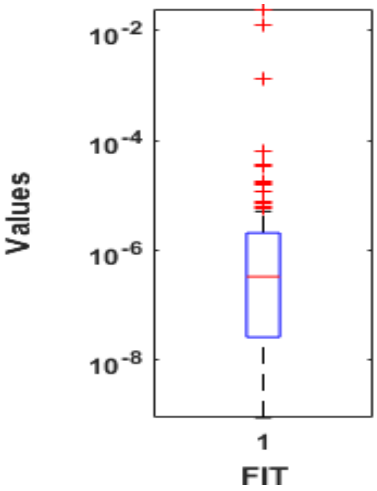

(f) Boxplot: Example 2

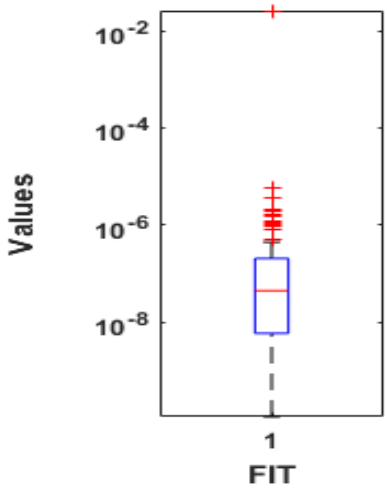

(g) Boxplot: Example 3

Figure 3. Statistical investigation via Fitness, histogram along with boxplots for the SO-LES-NM using the GNN-PSO-SQPS.

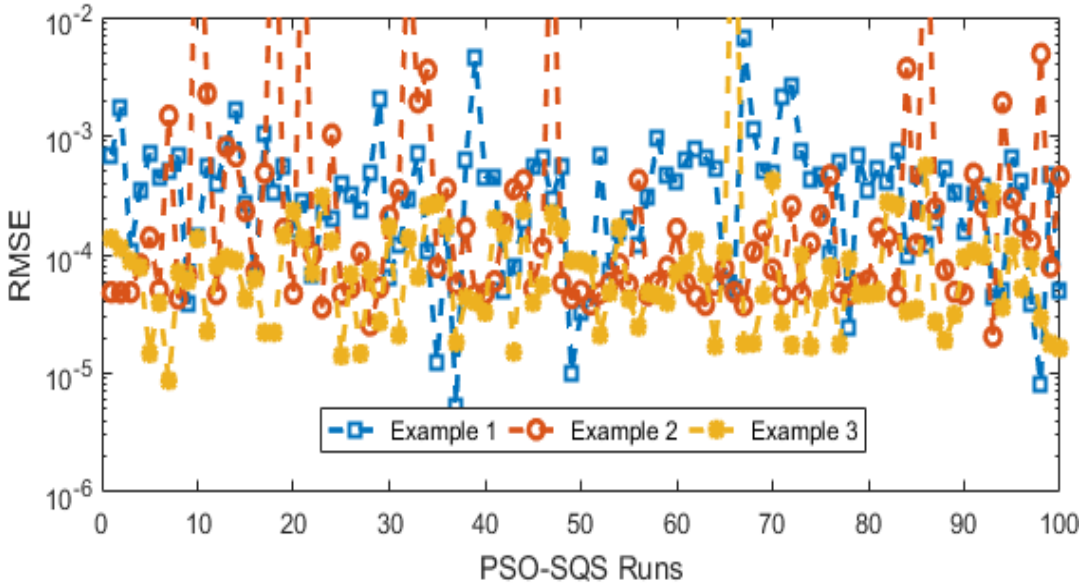

(a) RMSE values using convergence investigations for Examples 1 to 3

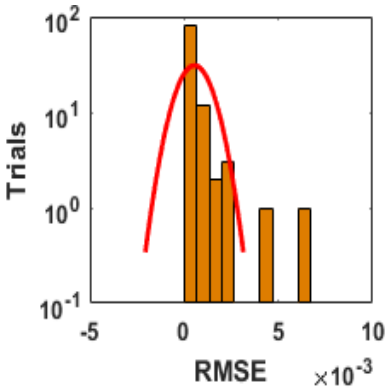

(b) Hist for Example 1

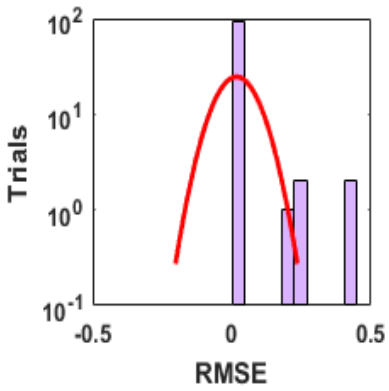

(c) Hist for Example 2

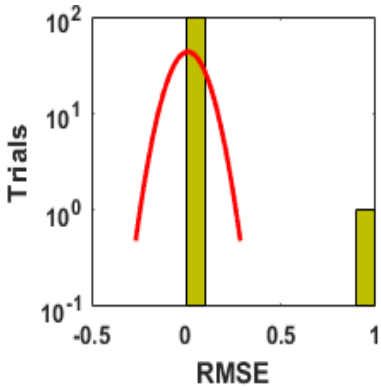

(d) Hist for Example 3

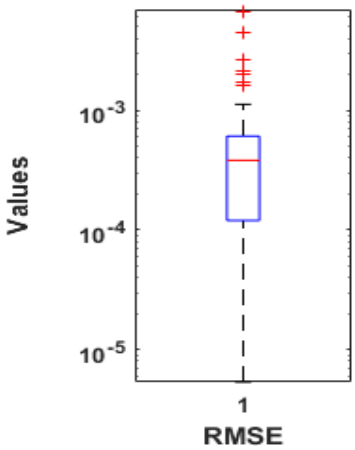

(e) Boxplot: Example 1

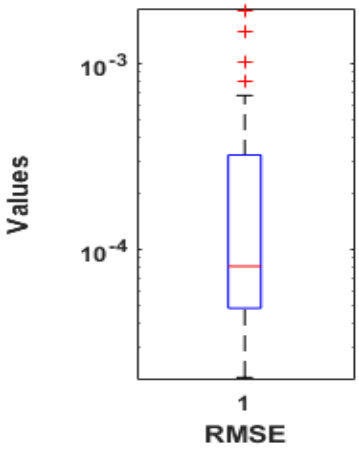

(f) Boxplot: Example 2

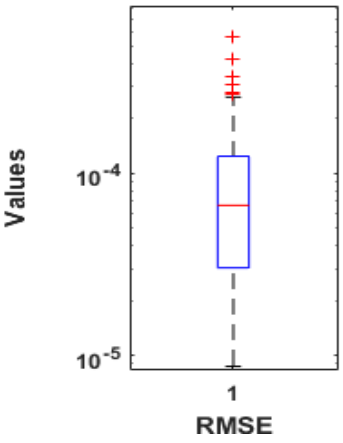

(g) Boxplot: **Example 3**

Figure 4. Statistical investigation via Fitness, histogram along with boxplots for the SO-LES-NM using the GNN-PSO-SQPS.

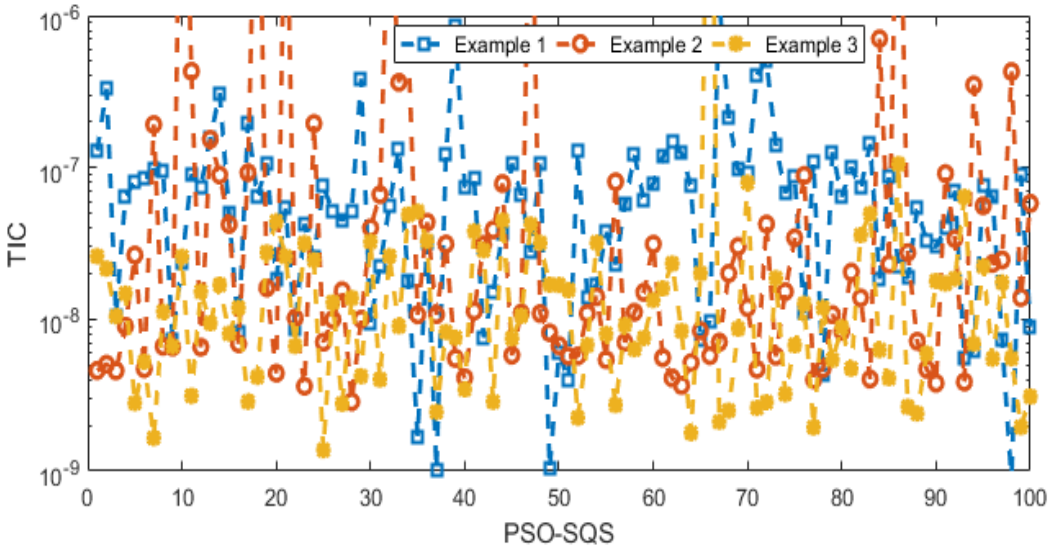

(a) TIC values using convergence investigations for Examples 1 to 3

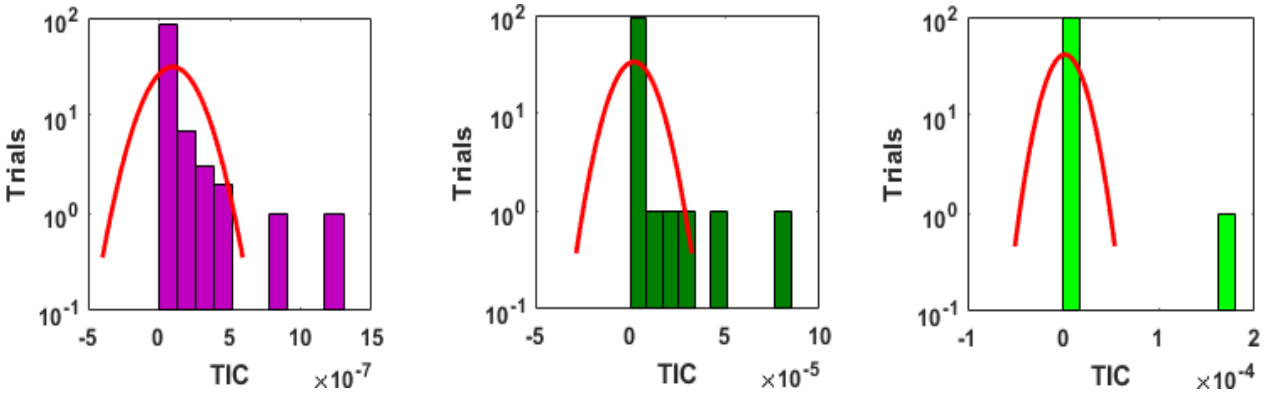

(b) Histfor Example 1

(c) Hist for Example 2

(d) Hist for Example 3

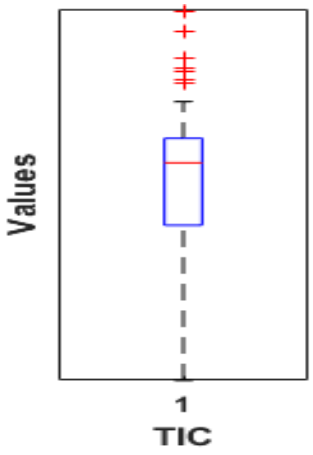

(e) Boxplot: Example 1

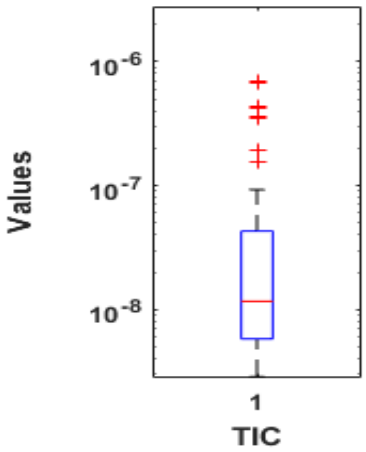

(f) Boxplot: Example 2

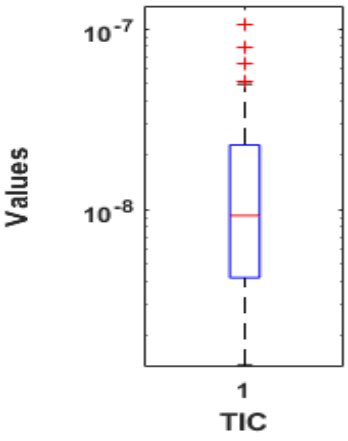

(g) Boxplot: Example 3

Figure 5. Statistical investigation via Fitness, histogram along with boxplots for the SO-LES-NM using GNN-PSO-SQPS.

Table 2. Statistical presentations for all examples of the SO-LES-NM using the designed GNN-PSO-SQPS.

Index	Gages	The outcomes through GNN-PSO-SQPS for the SO-LES-NM										
		0	0.10	0.20	0.30	0.40	0.50	0.60	0.70	0.80	0.90	1.0
E 1	Min	1×10^{-07}	5×10^{-06}	5×10^{-06}	6×10^{-06}	7×10^{-08}	2×10^{-06}	6×10^{-06}	5×10^{-06}	5×10^{-06}	4×10^{-06}	3×10^{-06}
	Mean	1×10^{-04}	2×10^{-04}	4×10^{-04}	6×10^{-04}	6×10^{-04}	6×10^{-04}	6×10^{-04}	6×10^{-04}	5×10^{-04}	4×10^{-04}	4×10^{-04}
	Max	2×10^{-03}	3×10^{-03}	5×10^{-03}	5×10^{-03}	7×10^{-03}	8×10^{-03}	9×10^{-03}	8×10^{-03}	8×10^{-03}	7×10^{-03}	6×10^{-03}
	Med	4×10^{-05}	1×10^{-04}	3×10^{-04}	4×10^{-04}	4×10^{-04}	4×10^{-04}	4×10^{-04}	4×10^{-04}	3×10^{-04}	2×10^{-04}	2×10^{-04}
	STD	3×10^{-04}	3×10^{-04}	6×10^{-04}	8×10^{-04}	1×10^{-03}	1×10^{-03}	1×10^{-03}	1×10^{-03}	9×10^{-04}	8×10^{-04}	7×10^{-04}
	S-I-R	5×10^{-05}	1×10^{-04}	2×10^{-04}	3×10^{-04}	2×10^{-04}	2×10^{-04}	2×10^{-04}	2×10^{-04}	2×10^{-04}	2×10^{-04}	2×10^{-04}
E 2	Min	1×10^{-06}	1×10^{-05}	1×10^{-05}	2×10^{-05}	1×10^{-05}	1×10^{-05}	1×10^{-05}	1×10^{-05}	1×10^{-05}	1×10^{-05}	1×10^{-05}
	Mean	2×10^{-02}	2×10^{-02}	2×10^{-02}	2×10^{-02}	1×10^{-02}	1×10^{-02}	1×10^{-02}	1×10^{-02}	8×10^{-03}	6×10^{-03}	4×10^{-03}
	Max	7×10^{-01}	7×10^{-01}	6×10^{-01}	5×10^{-01}	4×10^{-01}	3×10^{-01}	2×10^{-01}	2×10^{-01}	2×10^{-01}	1×10^{-01}	1×10^{-01}
	Med	1×10^{-04}	1×10^{-04}	9×10^{-05}	7×10^{-05}	8×10^{-05}	8×10^{-05}	8×10^{-05}	7×10^{-05}	6×10^{-05}	5×10^{-05}	4×10^{-05}
	STD	1×10^{-01}	1×10^{-01}	1×10^{-01}	8×10^{-02}	7×10^{-02}	6×10^{-02}	5×10^{-02}	4×10^{-02}	3×10^{-02}	2×10^{-02}	2×10^{-02}
	S-I-R	1×10^{-04}	1×10^{-04}	1×10^{-04}	$1\times10_{-04}$	1×10^{-04}	1×10^{-04}	1×10^{-04}	1×10^{-04}	8×10^{-05}	6×10^{-05}	4×10^{-05}
E 3	Min	7×10^{-08}	2×10^{-07}	2×10^{-06}	8×10^{-07}	1×10^{-07}	8×10^{-07}	6×10^{-08}	1×10^{-06}	2×10^{-07}	1×10^{-06}	1×10^{-10}
	Mean	2×10^{-02}	1×10^{-02}	1×10^{-02}	8×10^{-03}	6×10^{-03}	5×10^{-03}	4×10^{-03}	3×10^{-03}	2×10^{-03}	1×10^{-03}	8×10^{-04}
	Max	2×10^{-01}	1×10^{-01}	1×10^{-01}	8×10^{-01}	6×10^{-01}	5×10^{-01}	4×10^{-01}	3×10^{-01}	2×10^{-01}	1×10^{-01}	8×10^{-02}
	Med	1×10^{-04}	9×10^{-05}	6×10^{-05}	5×10^{-05}	5×10^{-05}	4×10^{-05}	4×10^{-05}	2×10^{-05}	1×10^{-05}	1×10^{-05}	1×10^{-06}
	STD	2×10^{-01}	1×10^{-01}	1×10^{-01}	8×10^{-02}	6×10^{-02}	5×10^{-02}	4×10^{-02}	3×10^{-02}	2×10^{-02}	1×10^{-02}	8×10^{-03}
	S-I-R	1×10^{-04}	6×10^{-05}	5×10^{-05}	3×10^{-05}	3×10^{-05}	2×10^{-05}	2×10^{-05}	2×10^{-05}	1×10^{-05}	9×10^{-06}	6×10^{-06}

Table 3. Global values for the SO-LES-NM using the designed GNN-PSO-SQPS.

Example	[G-FIT]		[G-RMSE]		[G-TIC]	
	Min	MED	Min	MED	Min	MED
1	1.00696E-10	7.28133E-07	5.36058E-06	3.81384E-04	8.66807E-10	6.33787E-08
2	9.02993E-10	3.33640E-07	2.04610E-05	8.11596E-05	2.86113E-09	1.16280E-08
3	1.14757E-08	4.48479E-08	8.71755E-06	6.65576E-05	1.37498E-09	9.27960E-09

Table 4. Complexity performances for the SO-LES-NM using the GNN-PSO-SQPS.

Example	Generation		Executed Time		Function Calculations	
	Mean	STD	Mean	STD	Mean	STD
1	32.341614	10.792954	1375.580000	1118.437060	48632.910000	15590.684384
2	38.944620	13.014598	1533.930000	1257.031988	57831.440000	18477.308549
3	35.375101	13.738706	1773.990000	1590.724900	53064.810000	19709.332159

4. Conclusions

The present research investigations are associated to present a novel Gudermannian neural network to solve the nonlinear second order singular Lane-Emden system using the hybrid

computing GNN-PSO-SQPS framework involving singularities at the origin. An error based objective function is optimized by using the global capability of particle swarm optimization and fast/rapid sequential quadratic scheme using 10 numbers of neurons throughout the present study. The design of the Gudermannian neural network is successfully exploited to solve the nonlinear second order singular Lane-Emden system. The obtained results using the process of optimization through the Gurmannian kernels have been compared with the true solutions for three different examples to check the precision and correctness of the suggested GNN-PSO-SQPS. One can find that the obtained and exact results overlapped over one another and examined the accuracy of order 5 to 7 decimal places. Furthermore, the performance of the scheme is investigated through the RMSE and TIC operators by taking the mean, worst and best AE values for all examples of the nonlinear second order singular Lane-Emden system. It is observed that the best values lie around 10^{-06}-10^{-08}, while the mean results and even the worst results lie in the good ranges for all the measures. The statistical clarifications for the 100 independent trials are implemented to the nonlinear second order singular Lane-Emden system in terms of the gages minimum, median, standard deviation, maximum, semi inter quartile range, mean authenticates the trustworthiness, robustness, accurateness and exactness of the proposed GNN-PSO-SQPS that is identified further by the performance measures of RMSE and TIC.

In the future, the considered GNN-PSO-SQPS can be used to the biological systems [52,53], as well as, two or three-dimensional systems of fluid dynamics [54–57].

Conflict of interest

The authors state that they have no conflict of interest. All authors have worked in an equal sense to find these results.

References

1. H. J. Lane, On the theoretical temperature of the Sun, under the Hypothesis of a gaseous Mass maintaining its Volume by its internal Heat and depending on the laws of gases as known to terrestrial Experiment, *Am. J. Sci.*, **148** (1870), 57–74.
2. R. Emden, Gaskugeln Teubner. Leipzig und Berlin, 1907.
3. Z. Sabir, H. A. Wahab, H. Umr, M. G. Sakar, M. A. Z. Raja, Novel design of Morlet wavelet neural network for solving second order Lane–Emden equation, *Math. Comput. Simul.*, **172** (2020), 1–14.
4. D. Baleanu, S. S. Sajjadi, A, Jajarmi, J. H. Asad, New features of the fractional Euler-Lagrange equations for a physical system within non-singular derivative operator. *Eur. Phys. J. Plus*, **134** (2019), 181.
5. T. Luo, Z. Xin, H. Zeng, Nonlinear asymptotic stability of the Lane-Emden solutions for the viscous gaseous star problem with degenerate density dependent viscosities, *Comm. Math. Phys*, **347** (2016), 657–702.
6. J. A. Khan, M. A. Z. Raja, M. M. Rashidi, M. I. Syam, A. M. Wazwaz, Nature-inspired computing approach for solving non-linear singular Emden–Fowler problem arising in electromagnetic theory, *Connect. Sci.*, **27** (2015), 377–396.
7. M. Ghergu, V. Rădulescu, On a class of singular Gierer-Meinhardt systems arising in morphogenesis, *C. R. Math.*, **344** (2007), 163–168.

8. R Rach, J. S. Duan, A. M. Wazwaz, Solving coupled Lane–Emden boundary value problems in catalytic diffusion reactions by the Adomian decomposition method, *J. Math. Chem.*, **52** (2014), 255–267.
9. A. H. Bhrawy, A. S. Alofi, R. A. Van Gorder, An efficient collocation method for a class of boundary value problems arising in mathematical physics and geometry, *Abst. Appl. Anal.*, **2014** (2014).
10. M. Dehghan, F. Shakeri, Solution of an integro-differential equation arising in oscillating magnetic fields using He's homotopy perturbation method, *Prog. Electromagn. Res.*, **78** (2008), 361–376.
11. D. Flockerzi, K. Sundmacher, On coupled Lane-Emden equations arising in dusty fluid models, *J. Phys.: Conference Series*, **268** (2011), 012006.
12. V. Rădulescu, D. Repovš, Combined effects in nonlinear problems arising in the study of anisotropic continuous media, *Nonlinear Anal. Theor. Methods Appl.*, **75** (2012), 1524–1530.
13. W. Adel, Z. Sabir, Solving a new design of nonlinear second-order Lane-Emden pantograph delay differential model via Bernoulli collocation method, *Eur. Phys. J. Plus*, **135** (2020), 427.
14. S. Mall, S. Chakraverty, Numerical solution of nonlinear singular initial value problems of Emden-Fowler type using Chebyshev Neural Network method, *Neurocomputing*, **149** (2015), 975–982.
15. S. Mall, S. Chakraverty, Chebyshev neural network based model for solving Lane–Emden type equations, *Appl. Math. Comput.*, **247** (2014), 100–114.
16. S. Mall, S. Chakraverty, Regression-based neural network training for the solution of ordinary differential equations, *Int. J. Math. Modell. Numer. Optim.*, **4** (2013), 136–149.
17. Z. Sabir, M. Umar, J. L. G. Guirao, M. Shoaib, M. A. Z. Raja, Integrated intelligent computing paradigm for nonlinear multi-singular third-order Emden-Fowler equation, Neural Comput. Appl., (2020). Available from: https://doi.org/10.1007/s00521-020-05187-w.
18. I Ahmad, H. Ilyas, A. Urooj, M. S. Aslam, M. Shoaib, M. A. Z. Raja, Novel applications of intelligent computing paradigms for the analysis of nonlinear reactive transport model of the fluid in soft tissues and microvessels, *Neural Comput. Appl.*, **31** (2019), 9041–9059.
19. Z. Sabir, F. Amin, D. Pohl, J. L. G. Guirao, Intelligence computing approach for solving second order system of Emden-Fowler model, *J. Intell. Fuzzy Syst.*, In press.
20. Z. Sabir, S. Saoud, M. A. Z. Raja, H. A. Wahab, A. Arbi, Heuristic computing technique for numerical solutions of nonlinear fourth order Emden-Fowler equation, *Math. Comput. Simul.*, **178** (2020), 534–548.
21. M. A. Z. Raja, J. Mehmood, Z. Sabir, A. K. Nasab, M. A. Manzar, Numerical solution of doubly singular nonlinear systems using neural networks-based integrated intelligent computing. *Neural Comput. Appl.*, **31** (2019), 793–812.
22. S. U. I. Ahmed, F. Faisal, M. Shoaib, M. A. Z. Raja, A new heuristic computational solver for nonlinear singular Thomas-Fermi system using evolutionary optimized cubic splines, *European Phys. J. Plus*, **135** (2020), 1–29.
23. Z. Sabir, M. A. Z. Raja, M. Umar, M. Shoaib, Design of neuro-swarming-based heuristics to solve the third-order nonlinear multi-singular Emden–Fowler equation, *Eur. Phys. J. Plus*, **135** (2020), 1–17.
24. M. Umar, M. A. Z. Raja, Z. Sabir, A. S. Alwabli, M. Shoaib, A stochastic computational intelligent solver for numerical treatment of mosquito dispersal model in a heterogeneous environment, *Eur. Phys. J. Plus*, **135** (2020), 1–23.

25. A. H. Bukhari, M. Sulaiman, M. A. Z. Raja, S. Islam, M. Shoaib, P. Kumam, Design of a hybrid NAR-RBFs neural network for nonlinear dusty plasma system, *Alex. Eng. J.*, **59** (2020), 3325–3345.
26. Z. Sabir, M. A. Z. Raja, M. Umar, M. Shoaib, Neuro-swarm intelligent computing to solve the second-order singular functional differential model, *Eur. Phys. J. Plus*, **135** (2020), 474.
27. Z Sabir, H. A. Wahab, M. Umar, F. Erdoğan, Stochastic numerical approach for solving second order nonlinear singular functional differential equation, *Appl. Math. Comput.*, **363** (2019), 124605.
28. M. A. Z. Raja, F. H. Shah, M. Tariq, I. Ahmad, Design of artificial neural network models optimized with sequential quadratic programming to study the dynamics of nonlinear Troesch's problem arising in plasma physics, *Neural Comput. Appl.*, **29** (2018), 83–109.
29. Z. Sabir, M. A. Manzar, M. A. Z. Raja, M. Sheraz, A. M. Wazwaz, Neuro-heuristics for nonlinear singular Thomas-Fermi systems, *Appl. Soft Comput.*, **65** (2018), 152–169.
30. M. Umar, Z. Sabir, F. Amin, J. L. G. Guirao, M. A. Z. Raja, Stochastic numerical technique for solving HIV infection model of CD4+ T cells, *Eur. Phys. J. Plus*, **135** (2020), 403.
31. M. Umar, Z. Sabir, M. A. Z. Raja, Intelligent computing for numerical treatment of nonlinear prey-predator models, *Appl. Soft Comput.*, **80** (2019), 506–524.
32. Z. Sabir, M. A. Z. Raja, J. L. G. Guirao, M. Shoaib, A neuro-swarming intelligence based computing for second order singular periodic nonlinear boundary value problems, (2020), Pre-print.
33. M. A. Z. Raja, U. Farooq, N. I. Chaudhary, A. M. Wazwaz, Stochastic numerical solver for nanofluidic problems containing multi-walled carbon nanotubes, *Appl. Soft Comput.*, **38** (2016), 561–586.
34. A. Mehmood, A. Zameer, S. H. Ling, M. A. Z. Raja, Design of neuro-computing paradigms for nonlinear nanofluidic systems of MHD Jeffery-Hamel flow, *J. Taiwan Institute Chem. Eng.*, **91** (2018), 57–85.
35. M. Umar, F. Amin, H. A. Wahab, D. Baleanu, Unsupervised constrained neural network modeling of boundary value corneal model for eye surgery, *Appl. Soft Comput.*, **85** (2019), 105826.
36. Z. Sabir, M. A. Z. Raja, M. Shoaib, J. F. G. Aguilar, FMNEICS: Fractional Meyer neuro-evolution-based intelligent computing solver for doubly singular multi-fractional order Lane-Emden system, *Comput. Appl. Math.*, **39** (2020), 1–18.
37. M. A. Z. Raja, A. Zameer, A. U. Khan, A. M. Wazwaz, A new numerical approach to solve Thomas–Fermi model of an atom using bio-inspired heuristics integrated with sequential quadratic programming, *Springer Plus*, **5** (2016), 1400.
38. Y. Shi, R. C. Eberhart, Empirical study of particle swarm optimization, *Proceedings of the 1999 congress on evolutionary computation-CEC99 (Cat. No. 99TH8406)*, 3, 1945–1950. IEEE, 1999.
39. Y. Shi, Particle swarm optimization: Developments, applications and resources, In: *Proceedings of the 2001 congress on evolutionary computation (IEEE Cat. No. 01TH8546)*, 1, 81–86. IEEE, 2001.
40. A. P., Engelbrecht, *Computational intelligence: an introduction*. John Wiley & Sons, 2007.
41. S. Kefi, N. Rokbani, P. Krömer, A. M. Alimi, Ant supervised by PSO and 2-opt algorithm, AS-PSO-2Opt, applied to traveling salesman problem. In: 2016 IEEE International Conference on Systems, Man, and Cybernetics (SMC) (004866–004871), 2016, IEEE.
42. A. Taieb, A. Ferdjouni, A new design of fuzzy logic controller optimized by PSO-SCSO applied to SFO-DTC induction motor drive, *Int. J. Elect. Comput. Eng.*, **10** (2020), 2088–8708.

43. Y. Ding, W. Zhang, L. Yu, K. Lu, The accuracy and efficiency of GA and PSO optimization schemes on estimating reaction kinetic parameters of biomass pyrolysis, *Energy*, **176** (2019), 582–588.
44. E. Keybondorian, A. Taherpour, A. Bemani, T. Hamule, Application of novel ANFIS-PSO approach to predict asphaltene precipitation, *Petrol. Sci. Technol.*, **36** (2018), 154–159.
45. N. Ghorbani, A. Kasaeian, A. Toopshekan, L. Bahrami, A. Maghami, Optimizing a hybrid wind-PV-battery system using GA-PSO and MOPSO for reducing cost and increasing reliability, *Energy*, **154** (2018), 581–591.
46. G. Wang, J. Guo, Y. Chen, Y. Li, Q. Xu, A PSO and BFO-based learning strategy applied to faster R-CNN for object detection in autonomous driving, *IEEE Access*, **7** (2019), 18840–18859.
47. K. Long, X. Wang, X. Gu, Multi-material topology optimization for the transient heat conduction problem using a sequential quadratic programming algorithm, *Eng. Optimiz.*, **50** (2018), 2091–2107.
48. S. Sun, Geometric optimization of radiative enclosures using sequential quadratic programming algorithm, *ES Energy Environ.*, **6** (2019), 57–68.
49. G. Torrisi, S. Grammatico, R. S. Smith, M. Morari, A variant to sequential quadratic programming for nonlinear model predictive control. In: *2016 IEEE 55th Conference on Decision and Control (CDC)*, 2814–2819. IEEE, 2016.
50. G. Singh, M. Rattan, S. S. Gill, N. Mittal, Hybridization of water wave optimization and sequential quadratic programming for cognitive radio system, *Soft Comput.*, **23** (2019), 7991–8011.
51. R. Hult, M. Zanon, G. Frison, S. Gros, P. Falcone, Experimental validation of a semi-distributed sequential quadratic programming method for optimal coordination of automated vehicles at intersections, *Optim. Contr. Appl. Met.*, **41** (2020), 1068–1096.
52. M. Umar, Z. Sabir, M. A. Z. Raja, M. Shoaib, M. Gupta, Y. G. Sánchez, A Stochastic Intelligent Computing with Neuro-Evolution Heuristics for Nonlinear SITR System of Novel COVID-19 Dynamics, *Symmetry*, **12** (2020), 1628.
53. T. N. Cheema, M. A. Z. Raja, I. Ahmad, S. Naz, H. Ilyas, M. Shoaib, Intelligent computing with Levenberg-Marquardt artificial neural networks for nonlinear system of COVID-19 epidemic model for future generation disease control, *Eur. Phys. J. Plus*, **135** (2020), 1–35.
54. M. Umar, Z. Sabir, I. Ali, H. A. Wahab, M. Shoaib, M. A. Z. Raja, The 3-D flow of Casson nanofluid over a stretched sheet with chemical reactions, velocity slip, thermal radiation and Brownian motion, *Therm. Sci.*, **24** (2020), 2929.
55. M. Shoaib, M. A. Z. Raja, M. T. Sabir, S. Islam, Z. Shah, P. Kumam, H. Alrabaiah, Numerical investigation for rotating flow of MHD hybrid nanofluid with thermal radiation over a stretching sheet, *Sci. Rep.*, **10** (2020), 1–15.
56. Z. Shah, M. A. Z. Raja, Y. M. Chu, W. A. Khan, M. Waqas, M. Shoaib, et al. Design of neural network based intelligent computing for neumerical treatment of unsteady 3D flow of Eyring-Powell magneto-nanofluidic model, *J. Mater. Res. Technol.*, **9** (2020), 14372–14387.

AIMS Press